Songklanakarin J. Sci. Technol.
38 (5), 485-493, Sep. - Oct. 2016

http://www.sjst.psu.ac.th

Original Article

Identification of material parameters for springback prediction using cyclic tension–compression test

Thaweesak Phongsai[1], Weerapong Julsri[1], Bunyong Chongthairungruang[1], Surasak Suranuntchai[1], Suwat Jirathearanat[3], and Vitoon Uthaisangsuk[2*]

[1] *Department of Tool and Materials Engineering,*

[2] *Department of Mechanical Engineering*
Faculty of Engineering, King Mongkut's University of Technology Thonburi, Thung Khru, Bangkok, 10140 Thailand.

[3] *National Metal and Materials Technology Centre, National Science and Technology Development Agency*
Khlong Luang, Pathum Thani, 12120 Thailand.

Received: 6 July 2015; Accepted: 20 January 2016

Abstract

In sheet metal forming process, springback is a critical problem for die makers, particularly in case of advanced high strength steels. Therefore, FE simulations were often used to calculate materials deformation behavior and the springback occurrence of formed sheet metals. Recently, the Yoshida–Uemori model, a kinematic hardening model, has shown great capability for describing the elastic recovery of a material. Nevertheless, determination of model parameters is sophisticated for industrial applications. In this work, an AHS steel grade JIS JSC780Y was investigated, in which tension–compression tests were carried out and the procedure of parameter identification was analyzed. Different fitting methods were examined and verified by evaluation of cyclic stress–strain responses obtained from simulations of 1–element model and experiments. The most appropriate parameter set was determined. Finally, hat shape forming test was performed and springback obtained by calculation and experiment was compared. It was found that the introduced procedure could be acceptably applied.

Keywords: high strength steel, springback, Yoshida-Uemori model, material parameters

1. Introduction

At present, production of automotive components have become very high competitive. Thus, part manufacturers require shorter time for developing dies. Besides, more accurate methods are needed in order to improve the quality of produced parts. For current automotive parts, advanced high strength (AHS) steel grades have been continuously introduced and employed so that both lightweight and higher strength characteristics are fulfilled. However, one great challenge of AHS steels in the forming process is the springback effect. It significantly affects the final shape of parts and can raise critical problems by the part assembly. To precisely describe this behavior of such steels is sophisticated. Die makers as well as researchers have paid much attention to prediction and compensation of the springback (Carden *et al.*, 2002; Gan *et al.*, 2004). In the industries, finite element (FE) simulation has been widely employed in support of springback description. Accuracies of the FE simulation results depend not only on forming process parameters like tools and binder geometries, contact conditions, but also on the choice of the material's constitutive model. The material model plays an important role for calculating deformation behavior of formed sheet metal, which greatly influences arising elastic recovery, residual stresses and corresponding springback. Different types of material constitutive laws such

* Corresponding author.
Email address: vitoon.uth@kmutt.ac.th

as isotropic hardening law, kinematic hardening law, mixed isotropic–kinematic hardening law (Hodge *et al.*, 1957), the Armstrong–Frederick hardening law (Armstrong *et al.*, 1966), and the Geng–Wagoner hardening law (Geng *et al.*, 2000) have been developed and extended for describing individual material behavior. The Yoshida–Uemori model (Yoshida *et al.*, 2002; Yoshida *et al.*, 2003) have been introduced for representing deformation behavior of large–strain cyclic plasticity and stress–strain responses at small scale re–yielding after large pre–strain. In the model, a backstress equation was defined in order to capture the transient Bauschinger effect. Eggertsen *et al.* (2009) investigated five different hardening models and compared resulted cyclic curves between simulations and experiments for various steel grades. It was shown that the Yoshida–Uemori model could well characterize the transient Bauschinger effect, permanent softening and work hardening stagnation of the materials.

For using the Yoshida–Uemori model, a cyclic materials testing is required. Under compression sheet specimens generally tend to buckle. Due to these difficulties, many testing methods have been developed to obtain the characteristic cyclic stress–strain curve; Yoshida *et al.* (2002) successfully bonded a few thin sheets of metal to provide a support for sheet specimen during in plane cyclic tension–compression test at large strain. Another kind of frequently used experiment is the bending test, as reported in Zhao *et al.* (2007), Mattiasson *et al.* (2006) and Yoshida *et al.* (1998). However, stress–strain curves could not be directly gathered from the experimental data of such bending tests. Furthermore, optimization methods have been often applied for obtaining precise material parameters. They are usually based on an inverse approach, in which appropriate algorithm enables a minimization between experimental observed variables and simulated ones; Yoshida *et al.* (2003) used an iterative multipoint approximation concept for minimizing differences between test and corresponding numerical results. This approach was verified by comparing simulated stress–strain curves using the constitutive model incorporating parameters identified from experimental cyclic bending curves. Collin *et al.* (2009) employed an inverse approach code in the SidoLo software, which offered the minimization in order to evaluate the Chaboche model parameters. In a recent study, Eggertsen *et al.* (2010) performed FE simulations of a three point cyclic bending test in the explicit code of LS–DYNA (LS–DYNA, 2007). Parameter identification of applied hardening model was done by means of the optimization code LS-OPT. Nevertheless, such optimization methods are still not suitable for industrial purposes.

The aim of this work was to introduce parameter determination procedures for the Yoshida–Uemori model by a simple fitting method. Cyclic tension–compression experiments were performed, in which a designed sample fixture installation for preventing buckling by spring force was used and a video extensometer was employed to measure the sample elongation. Subsequently, cyclic stress–strain curves were determined and each parameter of the Yoshida–Uemori model was identified. Different obtained sets of parameters were evaluated by comparing the stress–strain responses from experiments and FE simulations of 1–element model. Finally, forming tests of a hat shape sample were carried out for verifying the parameter sets.

2. Yoshida–Uemori Hardening Model and Generalized Parameter Identification

The Yoshida-Uemori (Y-U) (Yoshida *et al.*, 2002) constitutive model takes into account both translation and expansion of the bounding surface (*F*), while the active yield surface (*f*) only evolves in a kinematic manner. A schematic of yield surfaces according to the Y-U model was presented in Chongthairungruang *et al.* (2013). *O* is the original center of the yield surface, β is the center of the bounding surface. α_* is the relative kinematic motion of the yield surface with respect to the bounding surface and can be expressed by

$$\boldsymbol{\alpha}_* = \boldsymbol{\alpha} - \boldsymbol{\beta} \tag{1}$$

$$\overset{\circ}{\boldsymbol{\alpha}}_* = C\left[\frac{a}{Y}(\boldsymbol{\sigma} - \boldsymbol{\alpha}) - \boldsymbol{\alpha}_*\sqrt{\frac{a}{\bar{\alpha}_*}}\right]\dot{\bar{\varepsilon}}_p \tag{2}$$

$$\dot{\bar{\varepsilon}}_p = \sqrt{\frac{2}{3}\boldsymbol{D}^p : \boldsymbol{D}^p}\,,\ \bar{\alpha}_* = \phi(\boldsymbol{\alpha}_*)\,,\ a = B + R - Y\,. \tag{3}$$

Y is the size of the yield surface and is constant throughout the deformation, *B*+*R* represents the size of the bounding surface and *B* is the initial size of bounding surface with *R* being associated with isotropic hardening. Uniaxial cyclic stress–strain curves described by the Y–U model were shown in Yoshida *et al.* (2002) for the yield and bounding surface. $\dot{\bar{\varepsilon}}_p$ is the effective plastic strain rate, which is defined as the second invariant of $\boldsymbol{D}^p$, and *C* is a material parameter that controls the rate of the kinematic hardening. Here, $(\circ)$ stands for the objective rate. The change of size and location for the bounding surface is defined as:

$$\dot{R} = k(R_{sat} - R)\dot{\bar{\varepsilon}}_p\,. \tag{4}$$

$$\overset{\circ}{\boldsymbol{\beta}}' = k\left(\frac{2}{3}b\boldsymbol{D}^p - \boldsymbol{\beta}'\dot{\bar{\varepsilon}}_p\right). \tag{5}$$

$$\sigma_{bound} = B + R + \beta\,. \tag{6}$$

$\boldsymbol{\beta}'$ and $\overset{\circ}{\boldsymbol{\beta}}'$ are the deviatoric component of $\boldsymbol{\beta}$ and its objective rate, respectively and *b* is a material parameter. The work hardening stagnation during reverse deformation, where *Y*, *C*, *B*, *k*, *b*, and R_{sat} are material constants were described in Yoshida *et al.* (2002). In addition, all parameters, except the parameter *h*, control the translation and expansion of the surface g_σ in Chongthairungruang *et al.* (2013). It could be used to fit the hardening stagnation behavior with experimental results. The Y–U model is referred to the kinematic hardening transversely anisotropic material model or the MAT_125 model in LS-DYNA.

Moreover, degradation of the elastic stiffness taking place during plastic loading could be considered by the Y–U model. It was found that varying elastic moduli should be defined for a simulation of the springback problem. The Young's modulus E was taken into account using following equation (Yoshida *et al.*, 2002).

$$E = E_0 - \left(E_0 - E_{sat}\right)\left[1 - exp\left(-\xi\bar{\varepsilon}_p\right)\right] \quad (7)$$

where E_0 and E_{sat} represent the Young's modulus value at initial state and infinitely large pre-strain state of material, respectively. ξ is a material constant.

The Yoshida–Uemori model involves overall seven material parameters, Y, C, B, R_{sat}, b, k, h. All of the parameters could be obtained from uniaxial stress–strain curve determined under a defined cyclic deformation, as depicted in Yoshida *et al.* (2002). A general approach for identifying each parameter was summarized as followed (Yoshida *et al.*, 2002). is the initial yield stress. It was determined as the elastic limit of material. The forward stress–strain curve (line (a)–(c)) in Yoshida *et al.* (2002) was fitted with the Equation 8. Then, the parameters B, k and term ($R_{sat} + b$) could be derived by this manner. A forward bounding surface curve $\sigma_{bound}^{(fow)}$ similar to the line (b)–(c) in Yoshida *et al.* (2002) was plotted.

$$\sigma_{bound}^{(fow)} = B + R + \beta = B + (R_{sat} + b)(1 - e^{-k\varepsilon^p}) \quad (8)$$

The parameter b represented the beginning of reverse bounding surface curve ($\sigma_{B0}^{(p)}$). It could be considered as the initial value at $\hat{\varepsilon}^p = 0$ of the reverse bounding surface curve. The reverse bounding surface curve was afore determined by extrapolating data of the reverse stress–strain curve from its saturation point, as line (e)-(j) illustrated in Yoshida *et al.* (2002). The difference between values at point (j) and (k) in Yoshida *et al.* (2002) was described by $\sigma_{B0}^{(p)}$. Since the parameter has been already derived, the parameter k could be directly identified using the experimentally obtained $\sigma_{B0}^{(p)}$ value and the relationship in Equation 9.

$$\sigma_{B0}^{(p)} = 2\beta_0 = 2b(1 - e^{-k\varepsilon_0^p}) \quad (9)$$

The parameter C is a material parameter, which controls the rate of the kinematic hardening. It was determined according to the range of transient Bauschinger deformation of the reverse stress–strain curve, as line (d)-(e) shown in Yoshida *et al.* (2002). The parameter C could be expressed as a function given in Equation 10.

$$C \approx \frac{2}{\hat{\varepsilon}^p}\left[\left(1 + ln2\right) - \sqrt{\frac{|\alpha_*|}{a}} + ln\left(1 + sgn(\alpha_*)\sqrt{\frac{|\alpha_*|}{a}}\right)\right] \quad (10)$$

The transient stress was defined as $\sigma_B^{(t)} = a + \alpha_*$ and $\frac{\alpha_*}{a}$ was in turn described as a function of the transient stress offset $\sigma_B^{(t)}$ as:

$$\frac{\alpha_*}{a} \approx \frac{\sigma_B^{(t)}}{a_0} - 1 = 2\left(\frac{\sigma_B^{(t)}}{\sigma_{B0}^{(t)}}\right) - 1 \ , \quad a_0 = \frac{1}{2}\sigma_{B0}^{(t)} = \sigma_0 - Y - \frac{1}{2}\sigma_{B0}^{(p)} \quad (11)$$

The parameter h is a material parameter, which demonstrates the expansion rate of non–isotropic hardening (non–IH surface), as shown in Chongthairungruang *et al.* (2013). It describes the rate of expansion of the surface g_σ . Larger values of the parameter h present a rapid expansion of non-IH surfaces, in which a prediction with lower saturated and smaller cyclic hardening was provided. Regarding Yoshida *et al.* (2002), this parameter was used for adjusting the calculated cyclic stress–strain curves to fit best with the experiment data. The value h ranges between 0 and 1.

3. Experiments

In this work, a dual phase (DP) steel sheet grade JIS JSC780Y with a thickness of 1.4 mm was investigated. Various material tests were performed in order to determine the mechanical behavior of the steel for parameters identification of the Yoshida–Uemori model. First, uniaxial tensile tests were carried out for obtaining anisotropic parameters of the DP steel. Determined mechanical properties of the investigated DP steel were given in Table 1.

A series of uniaxial tests were conducted for sheet samples taken in parallel to the rolling direction in order to investigate variations of the elastic modulus at different pre–

Table 1. Mechanical properties of the investigated steel obtained by tensile test and parameters for relationship between elastic modulus and pre–deformation.

Direction	E	σ_y	σ_u	Elongation (%)		r -value	Poisson's Ratio (assumed)
	(GPa)	(MPa)	(MPa)	Uniform	Total		
0°	199.852	457.804	809.673	14.122	23.894	0.9987	0.3
45°	187.057	459.780	805.465	15.119	27.019	1.1508	0.3
90°	219.998	469.094	819.639	14.561	24.576	1.1116	0.3

E_0 (GPa)	E_{sat} (GPa)	ξ
199.852	168.625	37.046

strain values. Uniaxial pre–deformation of about 0.02 was applied before and followed with unloading. Subsequently, an additional strain of 0.02 was introduced to the same sample and again succeeded with unloading. This procedure was repeated with an incremental strain of 0.02 until a total pre-strain of 0.1 was reached. The determined true stress–strain curves were plotted together, as shown in Figure 1a. From the determined true stress–strain curves, elastic moduli for each pre–strain were identified. Then, relationships between the elastic modulus and effective plastic strain were established with regard to Equation 7. The evolutions of the elastic modulus during plastic deformation experimentally obtained and calculated by Equation 7 are illustrated in Figure 1b. The involved parameters of the elastic modulus change were the initial elastic modulus E_0, saturated elastic modulus E_{sat} and material constant ξ, which are presented in Table 1.

Cyclic tension–compression tests were performed in order to obtain cyclic stress–strain curves for identifying material hardening parameters of the Yoshida–Uemori model. During the cyclic tests, a buckling of tested sheet specimens could occur. Thus, a specific tool installation was initially designed for the cyclic test in order to prevent the buckling problem. Kuwabara (2007) proposed a buckling prevention tool for thin sheet copper and aluminum alloy by using hydraulic system. A hard Teflon film was used for reducing friction between sheet specimens and clamping plates. In this work, spring forces were used instead for supporting the sheet specimens during tension–compression movement. In order to minimize the buckling effect and obtain optimum clamping force, array and number of spring needed to be specified. The spring grade SWF 12-50 with a spring constant k of 73.5 N/mm was finally selected for the fixture. This fixture included eight springs for supporting both clamping plates and exhibited the array in a serial pattern. By this installation, a pre-load of around 1,970 N and a maximum pressure of 1.58 MPa were realized. Almost no buckling was observed by the cyclic tests using this fixture installation.

By the tests, specimens were tensioned up to a total strain of about 7-11% in order to achieve a saturation of determined stress-strain curve. Afterwards, they were compressed until the plastic strain became zero. During the experiments, local displacements were measured by an advanced video extensometer (AVE) system. Figure 2 presents the gathered cyclic stress–strain curve under tension–compression load in comparison with stress–strain curve from monotonic tensile test. A fair agreement in the tension region of both stress–strain curves could be observed. The saturated zone of each cyclic curve could be identified by means of relation between strain hardening ($\frac{d\sigma}{d\varepsilon}$) and true strain. The strain hardening of material continuously decreased until reaching a constant state. Within this stress range model parameters were determined.

A stamping test of a hat-shape sample was carried out to verify the determined model parameters. The dimensions of die and punch were described in detail in Chongthairungruang *et al.* (2013). The initial size of the blank sheet was 50 mm in width, 314 mm in length, and 1.4 mm in thickness. The clearance of 7% of the sheet thickness was designed for the dies. In the forming process, a metal plate with a thickness of 1.6 mm or so–called dummy plates were used in order to inhibit blank holder force. After the forming tests, final

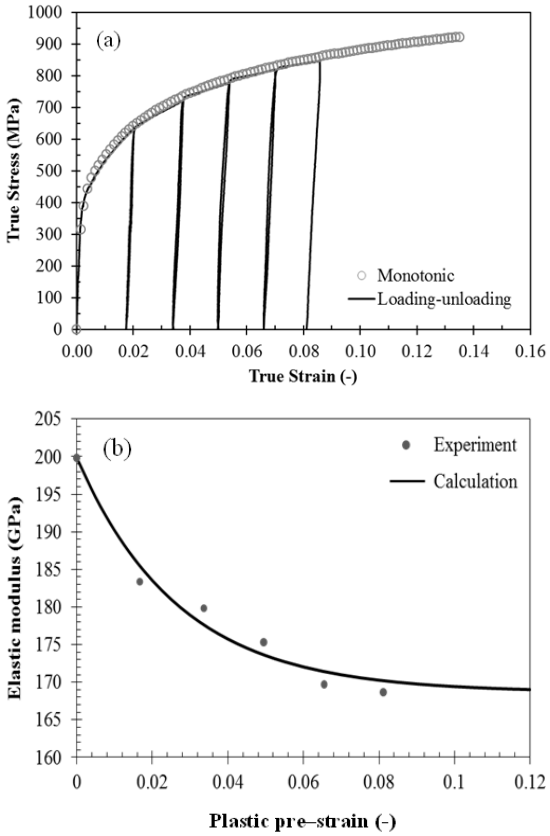

Figure 1. (a) True stress-strain curves from loading-unloading tensile test for investigating elastic modulus change and (b) dependency between elastic modulus and effective plastic strain of the investigated steel.

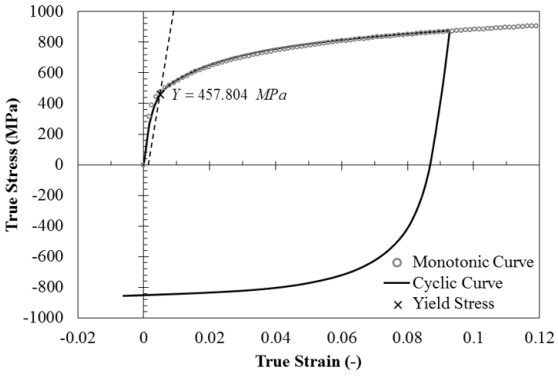

Figure 2. Comparison between experimentally obtained cyclic stress–strain curve under tension-compression load and monotonic tension stress–strain curve.

dimensions of stamped parts were measured using a 3D laser scanner. Shapes of the formed samples along cross–section after tool removal were considered for springback evaluation. The springback and sidewall curl were characterized by using three variables, the angles θ_1 and θ_2 and curl radius R.

4. Determination of Model Parameters

The Yoshida–Uemori hardening model used two sets of parameter for describing material behavior. These both parameter sets are presented as following.

a) Parameters representing relationship between Young's modulus and degree of pre–strain. This parameter set consists of E_0, E_a and ξ

b) Parameters representing plastic behavior of material. This parameter set includes seven parameters, namely, Y, C, B, R_{sat}, b, k, and h.

The parameters for elastic behavior were determined by interrupted tensile tests with various pre–strains as mentioned before. Determination of the plastic parameters is discussed here. Regarding constitutive equations of the Y–U model, the plastic parameters are dependent. Therefore, each parameter could not be identified individually or varied without any effect on other parameters. Thus, in this work, a simply method was introduced for determining sets of parameters and investigating their influences on cyclic stress–strain curves. This procedure could be applied in general without any further optimization method. The determination procedure could be presented in detail as following.

4.1 Parameter

Principally, the parameter Y is the material yield stress and could be determined by a standard method. The 0.2% offset strain was used to define the elastic limit. Figure 2 showed this elastic limit or yield strength of the investigated JSC780Y steel in comparison with the monotonic and cyclic curve.

4.2 Parameters from forward stress

Here, from the cyclic experiments, stress–strain data of the plastic zone beginning with the parameter Y were used. This plastic stress–strain curve under tension and compression were used to define the forward and reverse bounding surface. The forward bound stress according to Equation 8 was related to the Voce hardening model, which could be expressed by the following equation:

$$\sigma_{iso}^{(Voce)} = B + (A)(1 - e^{-k\varepsilon^p}) \quad (12)$$

where $A = R_{sat} + b$. Therefore, a forward bound curve could be simply described by Equation 12. However, ranges of data, which were used for curve fitting, strongly affected the variation of obtained parameter values. In this work, three ranges of data, namely, 50%, 75%, and 100% of the total forward plastic strain ε_0^p were considered for finding the parameter set, as illustrated in Figure 3a. From these ranges of data, three different sets of parameter were determined from the forward bound stress as following.

50% range of ε_0^p :

$$\sigma_{iso}^{(Voce)} = 608.095 + (355.647)(1 - e^{-15.872\varepsilon^p})$$

75% range of ε_0^p :

$$\sigma_{iso}^{(Voce)} = 565.676 + (367.699)(1 - e^{-20.755\varepsilon^p})$$

100% range of ε_0^p :

$$\sigma_{iso}^{(Voce)} = 489.528 + (399.003)(1 - e^{-32.330\varepsilon^p})$$

4.3 Parameters from reverse stress

The point (d) in Yoshida *et al.* (2002) represented a re–yielding point during compression, which was two times the elastic limit or $2Y$. Only the plastic zone of the reverse stress was taken into account, thus the reverse stress curve was plotted backwards to the plastic strain ε_0^p of 0.088. In addition, point (k) exhibited an isotropic boundary, for

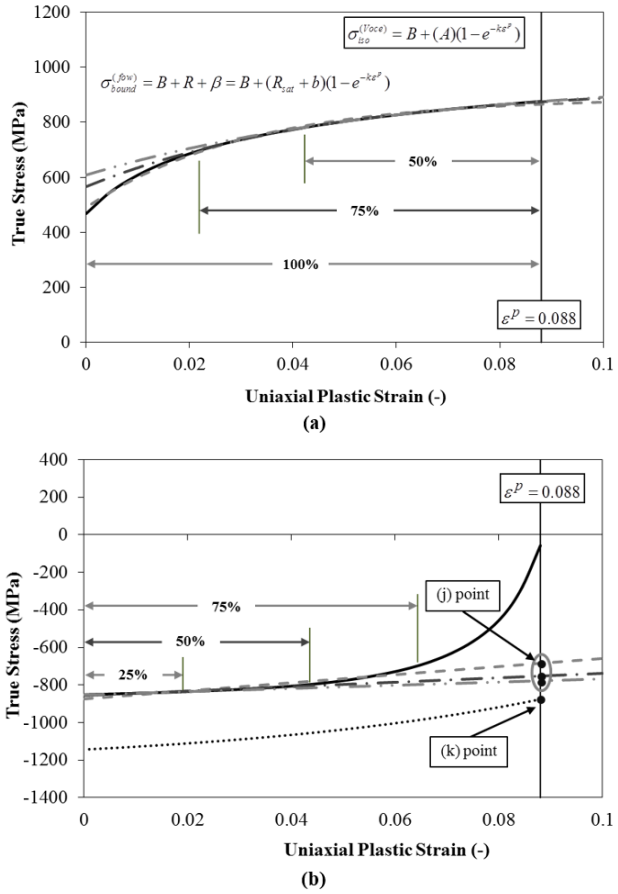

Figure 3. (a) Fitting of forward bound stress curve using different ranges of data (50%, 75%, and 100% of the total forward plastic strain) and (b) fitting of reverse bound stress curve using different ranges of data (25%, 50%, and 75% of the total reverse plastic strain).

which value of the forward stress at a plastic strain of 0.088 was used. For the investigated steel, the value of point (k) was about -876.12 MPa. Then, point (j) could be identified by an intersection of a linear extrapolation of the saturated reverse stress with the plastic strain of 0.088. Three ranges of data of the reverse bound curve from the saturated point were incorporated, namely, 25%, 50%, and 75% of the total reverse plastic strain, as shown in Figure 3b.

Following this, three values of point (j) in Yoshida *et al.* (2002) were obtained for these different ranges of data:

25% range of ε_0^p : value of point (j) was -777.87 MPa

50% range of ε_0^p : value of point (j) was -752.36 MPa

75% range of ε_0^p : value of point (j) was -684.71 MPa

Furthermore, the extrapolated line up to a deviation point of the reverse bound curve represented the region of permanent softening. The extrapolated line beyond this region until the total plastic strain described the transient Bauschinger effect. They were used in conjunction with Equation 9 to calculate the parameter *b*.

4.4 Parameter

Generally, in some literatures the parameter *C* was determined by an optimization method. Such kind of method was sophisticated and expensive for industrial cases. On the other hand, solving for *C* from Equation 10 and 11 could be another possibility. However, in this work more simple method for finding the parameter *C* was applied. The original backstress model as defined in Equation 13 was here considered.

$$\dot{\alpha}_* = C(a\dot{\varepsilon}^p - \alpha_* \left|\dot{\varepsilon}^p\right|) \tag{13}$$

This was the principle equation before it was modified by Yoshida *et al.* (2002) to be Equation 2. Thus, the value of *C* was then determined by a relation between cyclic tension–compression test data and parameter, as expressed in Equation 14.

$$\sigma_B^{(t)} \approx 2ae^{-C\hat{\varepsilon}^p} \tag{14}$$

where $\sigma_B^{(t)}$ described the differences between the reverse stress-strain curve from the range (d)-(e) and the extrapolated line of the transient Bauschinger region ((e)-(j)) in Yoshida *et al.* (2002). $\hat{\varepsilon}^p$ is the reverse plastic strain. Figure 4 shows the proposed method for determining the parameter *C*. By this manner, a value of 92.037 was obtained for the parameter *C*. It was noticed that stress–strain curves obtained by this value in the transient Bauschinger zone was acceptable when comparing with experimental results.

4.5 Parameter *h*

In the literature, *h* is a material parameter, which was used to adjust results of cyclic stress–strain curves obtained from experiments and simulations. In this work, it was found that influence of the parameter *h* on the results of cyclic simulations was small in the LS-DYNA solver. Therefore, a default value of $h = 0.5$ was taken into account.

From the procedures mentioned above, various parameter sets were obtained and provided in Table 2. All seven plastic parameters of the Y–U model for each range of fitting data were presented. It was seen that the parameters could be quite different when the range of fitting data was varied. These parameter sets were further applied for FE simulations of 1–element model in order to investigate their effects on cyclic stress–strain responses.

5. FE Simulations

5.1 1-element model

FE simulations of tension–compression test were performed in LS-DYNA by using a single plane stress shell element model. The model was a square element with a size of 1x1 mm. The left–bottom node was constrained in both x– and y–direction, while the right–bottom node was constrained in the y–direction. Displacements in positive and

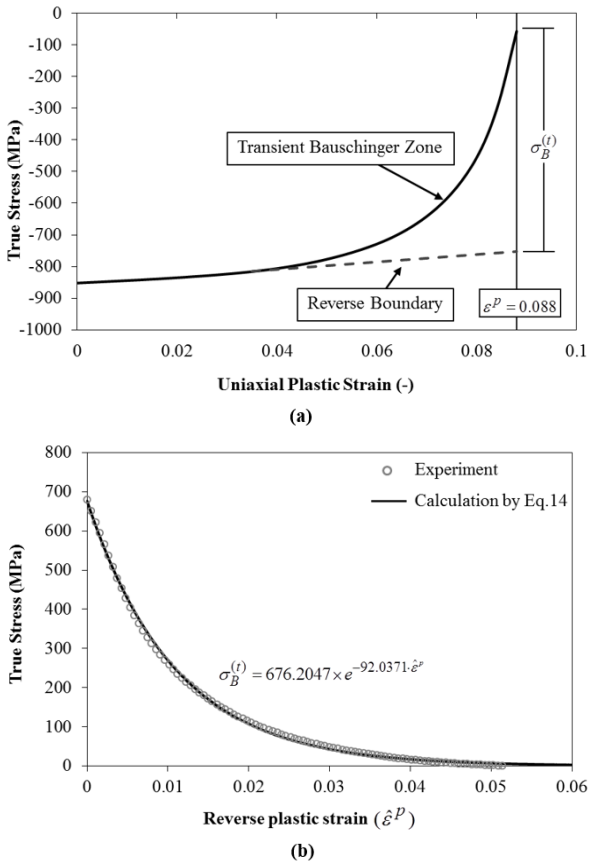

Figure 4. Determination of parameter *C*: (a) $\sigma_B^{(t)}$ and (b) curve fitting by Equation 14.

Table 2. Determined parameter sets for the investigated JSC780Y steel.

Range of fitting data		Parameters						
Forward stress	Reverse stress	Y	B	k	b	R_{sat}	C	h
50%	25% (A)	457.804	608.095	15.872	65.277	290.370	84.830	0.5
	50% (B)		608.095	15.872	82.222	273.425	92.037	
	75% (C)		608.095	15.872	127.170	228.478	113.746	
75%	25% (D)		565.676	20.755	58.553	309.146	84.830	
	50% (E)		565.676	20.755	73.753	293.947	92.037	
	75% (F)		565.676	20.755	114.070	253.629	113.746	
100%	25% (G)		489.528	32.330	52.159	346.844	84.830	
	50% (H)		489.528	32.330	65.699	333.304	92.037	
	75% (I)		489.528	32.330	101.613	297.390	113.746	

negative y–direction were applied to the top side of the element. The element formulation type 2 (Belytschko-Tsay) with one integration point through thickness was used. This element type was also further applied in forming simulations. Results of the each parameter set were compared with experimental data. Afterwards, averaged deviations between both obtained stress–strain curves were calculated.

5.2 Forming simulation

In addition, numerical FE simulations of the hat–shape sample were carried out in LS-DYNA for predicting the springback effect. It was also used to verify springback results of the parameter set, which was the best fit prediction of the cyclic stress–strain responses. The models of blank and tools were defined using shell elements and boundary conditions were generated according to the experimental setup. A friction coefficient of 0.125 was given for every contact surface. Calculated results were compared with the shape of the stamped part.

6. Results and Discussion

6.1 Cyclic stress–strain curves

To investigate influences of using different range of fitting data, 1–element FE simulations were conducted with all parameter sets, given in Table 2. Some deviations of stress–strain curves from each parameter sets were observed. The cyclic curves mainly differed at the beginning zone of forward stress and around the saturation zone of reverse stress. When the data range of the forward stress was the same, but the data range of the reverse stress increased, increases of the stress–strain curves in both tension and compression regions were found. The whole cyclic curves seemed to shift when only parameters from the reverse stress were altered. In case of using an increased data range of the forward stress, but the same data range of the reverse stress, decreases of the forward stress were observed. Additionally, the calculated curves were compared with the experimental ones for an entire cycle and errors of each case were then determined. The mean differences and standard deviations for each parameter sets were summarized in Table 3. It was found that the range of fitting data, which provided the best agreement with the experimental data, was the 50% range of ε_0^p from the forward stress in combination with the 75% range of ε_0^p from the reverse stress (case C). The largest difference value was noticed by the 75% range of ε_0^p from the forward stress and the 25% range of ε_0^p from the reverse stress (case D). The cyclic stress–strain curves of both parameter sets were compared with the experimental curve in Figure 5. The worst parameter set exhibited significant lower forward stress, lower reverse stress in the range of permanent softening and higher reverse stress in the transient Bauschinger region. For the best parameter set, a maximum stress difference of 20 MPa was detected.

6.2 Springback results

To verify springback effects predicted by the Y–U model using the determined parameters, FE simulations of hat–shape samples were carried out. Both parameter sets discussed before were applied to the simulations to investigate influences of model parameters on the calculated springback. Experimental and simulation results regarding both designated angles θ_1 and θ_2, and sidewall curl radius R were determined. In Figure 6, dimensions of stamped parts obtained from the experiment and predicted by the simulations using two different parameter sets were compared. All three springback variables obtained from the experiments and predicted by the simulations were compared with resulted %-error in Figure 7. The calculated springback results of both parameter sets were similar and slightly different from the experimental one. Nevertheless, the error of the best fit parameter set was slightly lower than the worst fit parameter set for every springback variable.

Table 3. Mean errors and standard deviations between simulations and experiments for each parameter set.

Range of fitting data		Error between simulation and experiment	
Forward stress	Reverse stress	Mean	S.D.
50%	25% (A)	35.9	20.6
	50% (B)	31.2	19.9
	75% (C)	20.7	19.5
75%	25% (D)	38.7	20.1
	50% (E)	34.4	19.0
	75% (F)	23.6	17.9
100%	25% (G)	38.5	22.5
	50% (H)	34.9	20.6
	75% (I)	25.9	17.6

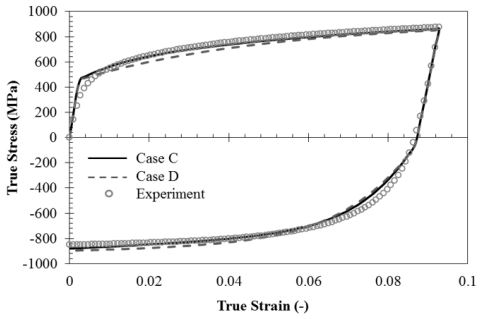

Figure 5. Comparison of stress–strain curves experimentally determined and calculated using the best fit and the worst fit parameter sets.

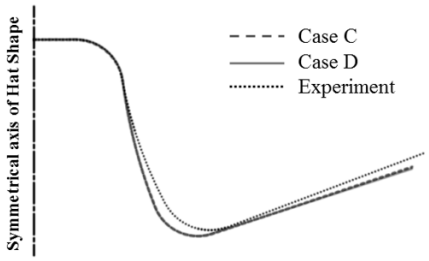

Figure 6. Shape comparison of stamped part determined by experiment and predicted by simulations applying two parameter sets.

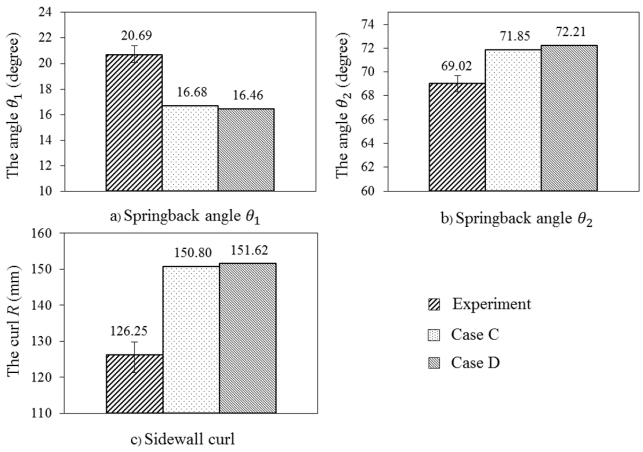

	% Error between experiment and simulation	
	parameter set C	parameeter set D
Springback angle θ_1	19.38	20.44
Springback angle θ_2	4.1	4.62
The sidewall curl R	19.44	20.1

Figure 7. Comparison of springback angles and sidewall curl radius of stamped parts measured by experiments and predicted by FE simulations and %-error.

7. Conclusions

In the current study, the Yoshida–Uemori model was used to investigate springback effect of the JSC780Y steel. This kinematic hardening model consists of seven plastic parameters. The simple approach for determining model parameters from cyclic tension–compression stress–strain curves was introduced in detail. Nevertheless, different parameter sets were obtained. Influences of these parameter sets on the predicted stress–strain responses were examined by means of 1–element FE simulations under tension–compression load. In addition, it was found that the determined parameters provided acceptable agreement with the experimental results. For verification of the parameters, stamping tests of the hat–shape sample were carried out. The calculated springback results of different parameter sets were similar and slightly different from the experiments. The error of the best fit parameter set was slightly lower than the worst fit parameter set for every springback variables. The recommended procedure for parameter determination of the Y–U model for the investigated steel is here summarized:

1) Parameter Y was identified as the 0.2% offset yield stress, 2) Forward bounding surface was obtained by fitting the 50% range of the forward stress data and using the Voce hardening model, 3) Reverse bounding surface was determined by fitting the 75% range of the reverse stress data and using a linear equation, and 4) Parameter C was identified by the differences between the reverse stress–strain curve and the extrapolated line of the transient Bauschinger region.

Acknowledgements

Authors would like to acknowledge the NSTDA University Industry Research Collaboration (NUI-RC) and the National Research University Project of Thailand's Office of the Higher Education Commission for financial support, the National Metal and Materials Technology Center (MTEC), National Science and Technology Development Agency of Thailand (NSTDA) and Iron and Steel Institute of Thailand (ISIT) for the materials testing, Thai Marujun Co., Ltd. and Chong Thai Rung Ruang Co., Ltd. for material support.

References

Armstrong, P.J. and Frederick, C.O. 1966. A mathematical representation of the multiaxial Bauschinger effect. G.E.G.B report RD/B/N 731

Carden, W.D., Geng, L.M., Matlock, D.K., and Wagoner, R.H. 2002. Measurement of springback. International Journal Mechanical Science. 44, 79-101.

Chongthairungruang, B., Uthaisangsuk, V., Suranuntchai, S., and Jiratheranat, S. 2013. Springback prediction in sheet metal forming of high strength steels. Material Design. 50, 253-266

Collin, J.M., Parenteau, T., Mauvoisin, G., and Pilvin, P. 2009. Material parameters identification using experimental continuous spherical indentation for cyclic hardening. Computational Materials Science. 46 (2), 333-338.

Eggertsen, P.A. and Mattiasson, K. 2010. On constitutive modeling of springback analysis. International Journal of Mechanical Science. 52, 804-818.

Eggertsen, P.A. and Mattiasson, K. 2009. On constitutive modeling of the bending-unbending behaviour for accurate springback predictions. International Journal of Mechanical Science. 51, 547-563.

Gan, W. and Wagoner, R.H. 2004. Die design method for sheet springback. International Journal of Mechanical Science. 46, 1097-113.

Geng, L. and Wagone, R.H. 2000. Springback analysis with a modified hardening model. SAE paper No. 2000-01-0768, SAE. Inc.

Hodge, P.G. 1957. A new method of analyzing stresses and strains in work hardening solids, Transactions of ASME. Journal of Applied Mechanics. 24, 482-483.

Kuwabara, T. 2007. Advances in Experiments on Metal Sheets and Tubes in Support of Constitutive Modeling and Forming Simulations. International Journal of Plasticity. 23, 385-419.

LS-DYNA, 2007. Keyword User's Manual Version 971 Vol. 2: Material Models, Livermore Software Technology Corporation, California. USA.

Mattiasson, O.E. and Enqvist, B.K. 2006. Identification of material hardening parameters by the three-point bending of metal sheets. International Journal of Mechanical Science. 48, 1525-1532.

Yoshida, F. and Uemori, T. 2002. A model of large-strain cyclic plasticity describing the Bauschinger effect and work hardening stagnation. International Journal of Plasticity. 18, 661-686.

Yoshida, F. and Uemori, T. 2003. A model of large-strain cyclic plasticity and its application to springback simulation. International Journal of Mechanical Science. 45, 1687-1702.

Yoshida, F., Uemori, T., and Fujiwara, K. 2002. Elastic-plastic behaviour of steel sheets under in-plane cyclic tension-compression at large strain. International Journal of Plasticity, 18, 633-659.

Yoshida, F., Urabe, M., and Toropov, V.V. 1998. Identification of material parameters in constitutive model for sheet metals from cyclic bending tests. International Journal of Mechanical Science. 40, 237-249.

Zhao, K.M. and Lee, J.K. 2007. Generation of cyclic stress-strain curves for sheet metals. Journal of Engineering Materials Technology. 38, 391-395.